

HARPO: a TPC as a gamma-ray telescope and polarimeter

Denis Bernard, Philippe Bruel, Mickael Frodin, Yannick Geerebaert, Berrie Giebels,
Philippe Gros, Deirdre Horan, Marc Louzir, Patrick Poilleux, Igor Semenouk, Shaobo Wang ^a

^aLLR, Ecole Polytechnique, CNRS/IN2P3, 91128 Palaiseau, France

Shebli Anvar, David Attié, Paul Colas, Alain Delbart, Patrick Sizun ^b

^bIRFU, CEA Saclay, 91191 Gif-sur-Yvette, France

Diego Götz ^{b,c}

^cAIM, CEA/DSM-CNRS-Université Paris Diderot, IRFU/Service d'Astrophysique,
CEA Saclay, F-91191 Gif-sur-Yvette, France

March 1, 2022

Paper No. 9144-57

**Presented at *SPIE Astronomical Telescopes + Instrumentation,*
Ultraviolet to gamma ray,
Palais des congrès de Montréal, Montréal, Québec, Canada; 22 - 27 June 2014**

Abstract

A gas Time Projection Chamber can be used for gamma-ray astronomy with excellent angular-precision and sensitivity to faint sources, and for polarimetry, through the measurement of photon conversion to e^+e^- pairs. We present the expected performance in simulations and the recent development of a demonstrator for tests in a polarized photon beam.

Keywords: gamma-ray, pair conversion, telescope, polarimeter, time projection chamber, tracking, Kalman filter, optimal variable, gaseous detector, micro-pattern gas detector, micromegas, gas electron multiplier.

1 INTRODUCTION

Several classes of cosmic sources such as active galactic nuclei (AGN), pulsars and gamma-ray bursts (GRB) produce huge flows of gamma rays. These high-energy photons are produced by non-thermal processes such as synchrotron radiation and inverse Compton scattering, and provide insight to understanding the structure of these sources and the emission mechanisms at work. In the 10 MeV – 100 GeV photon energy range, telescopes on space missions have been using the gamma conversion to e^+e^- pairs in high- Z converters which are interleaved with particle trackers, to detect astrophysical sources.

1.1 Angular resolution

The successive COS-B, EGRET, AGILE and Fermi missions have shown an impressive improvement in the effective area and in sensitivity, but hopes for high sensitivity at low energy (e.g. Ref. [1]) have been unfulfilled: even the Fermi-LAT is actually publishing results mainly above 100 MeV. Fermi is sensitive down to 20 MeV, as is demonstrated by GRB analyses, for which a loose event selection is possible because

of the small integration time. But for standard analyses with a long integration time, a much more stringent selection is required, which affects the effective area below 1 GeV: the effective area is one order of magnitude smaller at 100 MeV than above 1 GeV (Fig 14 of Ref. [2]). The other key issue at low energy is the strong degradation of the angular resolution, which makes source finding very difficult, especially in crowded regions of the sky such as the galactic plane. The Fermi-LAT differential sensitivity at 100 MeV for class P7SOURCE_V6 for a point source for a 3-year exposure, 4 bins per energy decade, with a 5σ sensitivity requirement and at least 10 counts per bin is $5 \times 10^{-6} \text{MeVcm}^{-2}\text{s}^{-1}$ for an “intermediate” galactic latitude. This figure, $2.4 \times 10^{-6} \text{MeVcm}^{-2}\text{s}^{-1}$, is of the same order of magnitude as that for EGRET (from Ref. [1]), after rescaling to the same duration and binning.

The 1 – 100 MeV sensitivity gap[1] between the Compton and the pair telescopes has triggered many developments. On the Compton side, projects aiming at an improvement in the sensitivity of a factor 10 – 30 w.r.t. Comptel are in progress [3, 4, 5]. This would bring us at the level of $\approx 10^{-5} \text{MeVcm}^{-2}\text{s}^{-1}$ at a few MeV. Bridging this improvement by a detector able to extend at low energy the excellent high-energy (GeV) sensitivity of the Fermi-LAT telescope ($\approx 10^{-6} \text{MeVcm}^{-2}\text{s}^{-1}$) is urgently needed.

1.2 Polarimetry

In contrast with thermal emission and hadronic interactions (which produce spin-zero π^0), the emission mechanisms mentioned above produce a radiation that is linearly polarized to some extent. Polarization measurements provide an important tool for understanding the physical processes in astrophysical sources.

GRBs are thought to be created either by the explosion of a hypernova or through the coalescence of two compact objects (e.g., neutron stars, white dwarfs, black holes). In the relativistic jets that are thus produced, synchrotron emission is thought to be the dominant emission process. Electrons are accelerated to near light speed by the relativistic shocks and, given the presence of a strong magnetic field [6], the degree of polarization of the photons emitted by these jets is expected to be very high. Polarization measurements of the emission will therefore provide information critical to distinguishing between the many emission models that exist for GRBs (see, for example, Refs. [7, 8, 9, 10]).

Another source class whose study should benefit from polarimetry studies is **AGN** and, in particular, the **blazar** subclass, which emits strongly in the MeV - GeV energy range. These systems have powerful jets with strong magnetic fields that are thought to contain a large portion of the energy reservoir of the jet and to play a key role in the variability that is characteristic of these objects. Blazars have two broad emission components; the first, at lower energies, is believed to be from synchrotron emission by electrons and positrons in the strong magnetic field of the jet. The origin of the second emission component at higher energies has been the subject of much theoretical modeling. The proposed models fall into two broad categories, namely, hadronic and leptonic models. In the leptonic models, the high-energy electrons and positrons that generate the synchrotron emission, also upscatter photons to higher energies via the inverse-Compton mechanism,. Recently Zhang *et al.* have extended their predictions to the polarization of X and gamma-ray emission of blazars to polarization [11]. Using the example of the blazar RX J0648.7+1516, they show that for the subclass of high-synchrotron-peaked (HSP) blazars, the fraction of linear polarization P in the X-ray band (2 – 10 keV) is high and similar in magnitude for leptonic and hadronic models, while in the γ band (30 – 200 MeV) it is predicted to be of the order of 70% for protons and to be completely washed out for electrons (their Fig. 5).

Gamma-ray polarimetry also turns out to be the most sensitive tool to test possible **Lorentz invariance violation** (LIV), considered in building a quantized theory of gravitation. Within the framework of an effective field theory, a birefringence effect of the vacuum is predicted [12]. The linear polarization direction would be rotated through an energy-dependent angle, due to different phase velocities for opposite helicities. This vacuum birefringence would rotate the polarization direction of monochromatic radiation, or could depolarize linearly polarized radiation composed of a spread of energies. Due to the quadratic dependence of the deviation angle on the photon energy, $\theta \propto E^2$, extending the polarization measurements from the presently available range covered by Compton polarimeters (0.1 - 1.0 MeV) to higher energies would lead

to an improved sensitivity to LIV.

2 HARPO: a TPC as a gamma-ray telescope and polarimeter

The HARPO (Hermetic ARgon POLarimeter) project aims at characterizing the time projection chamber (TPC) technology as a high angular resolution and polarimeter telescope in the MeV - GeV energy range.

2.1 Angular resolution

The reconstruction of the incident direction of a photon that converts in a detector is affected by a series of effects that contribute to the angular resolution.

- **Multiple scattering.** The main factor affecting the lowest part of the energy range considered here is multiple scattering of the conversion electrons. Based on earlier works by Gluckstern [13] and Innes [14] on the determination of track parameters with optimal fits in the presence of multiple scattering, we have obtained [15] a parametrization of this (RMS) contribution as:

$$\sigma_\theta \approx (2\sigma)^{1/4} l^{1/8} X_0^{-3/8} (E/p_0)^{-3/4}. \quad (1)$$

where E is the photon energy, $p_0 = 13.6 \text{ MeV}/c$ is the usual multiple scattering parameter, X_0 is the radiation length of the TPC material and σ and l are the single point space resolution and the sampling pitch of the TPC, respectively. In deriving this expression we have neglected the small logarithmic correction factor that occurs in the expression for the multiple scattering angle (eq. (30.15) of Ref. [16]). Also an additional factor, close to unity, that arises in the computation of this contribution to the photon resolution, from the expression for each of the two tracks, is neglected (Fig 1 of Ref. [15]). We have validated [17] the effectiveness of such optimal fits fitting the track with a Kalman filter, using the prescriptions of Ref.[18], see Fig. 2 left. The $E^{-3/4}$ dependance of σ_θ (eq. (1)) can be compared to what has been observed experimentally, for example $E^{-0.78}$ for the Fermi-LAT [2].

- **Nucleus recoil.** In the case of photon conversion in the field of a nucleus, the path length of the recoiling nucleus in the detector is extremely short and its direction can't be measured. That missing contribution to the photon momentum induces a contribution to the angular resolution. Our study [15] shows that while the most probable angular shift varies like E^{-2} and becomes negligible above a few MeV, the increase of the fraction of events in the high recoil tail above the most probable value gives a different dependance to the the 68% containment angle, θ_{68} , which is the relevant figure in astronomy. We have discovered [15] that θ_{68} varies like $E^{-5/4}$.

As a consequence of the stronger E dependance, the kinematic limit dominates just above threshold, while multiple scattering dominates at intermediate energies. This is shown on Fig. 1 left. The plot shows the angular resolution for a point resolution $\sigma = 0.1 \text{ mm}$ and a sampling $l = 1.0 \text{ mm}$, for various TPC material (neon, argon, xenon) and densities (1 or 10 bar gas, liquid (Ar, Xe) or solid (Ne)). We see that in most of the energy range, an improvement of the angular resolution by more than one order of magnitude is within reach with respect to the Fermi-LAT (thicker black lines for “front” and “back” events [2]).

2.2 Conversion efficiency, effective area

In contrast with a “thick” detector, in which the probability of photon conversion is close to unity, in the present case of a “thin” detector, the efficiency is much smaller. But the relevant criterion is the effective area which is here proportional to the sensitive mass and to the photon attenuation and that is not that small (larger than $1 \text{ m}^2/\text{t}$ above 10 MeV for argon). A gaseous detector in orbit will certainly contain less

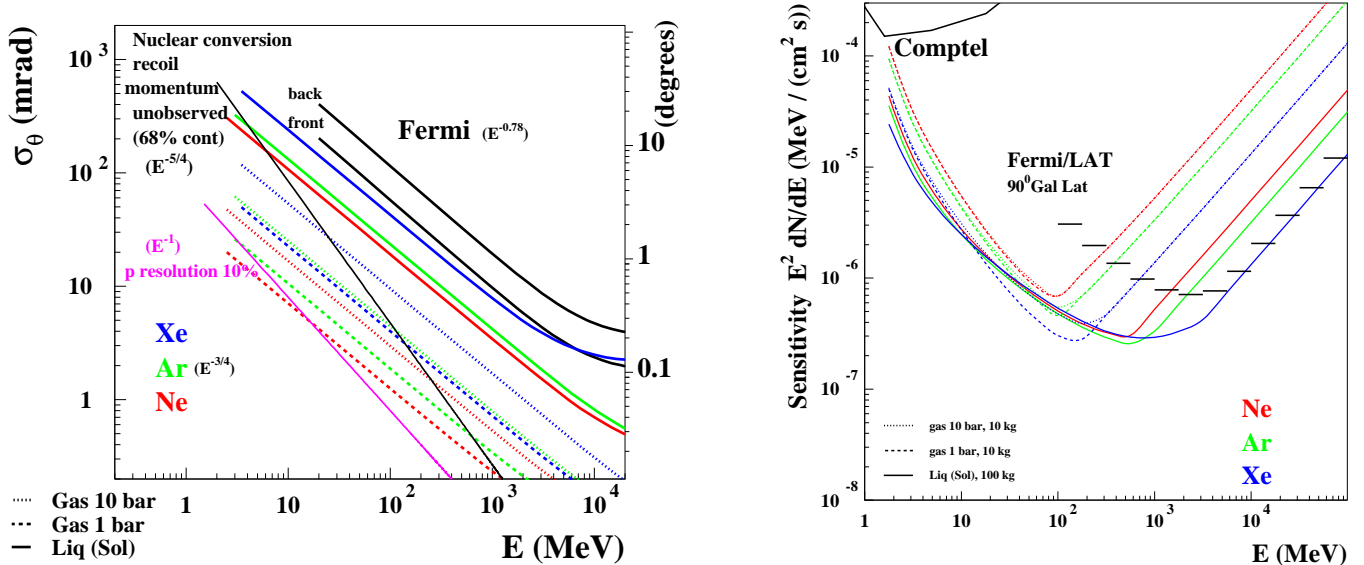


Figure 1: Left: Various contributions to the photon angular resolution. [15]. Right: Variation of the differential sensitivity as a function of energy [15] compared to the 90° galactic latitude performance of the Fermi-LAT [2] and of the Compton telescope COMPTEL [1].

than a ton of sensitive material (17 kg/m^3 for argon at 10 bar), but the point-like source sensitivity turns out to be better than that of the Fermi-LAT in the range $3 - 300 \text{ MeV}$ for a gas detector (Fig. 1 right and Ref. [15]). We see that a 10 kg gas TPC and a 100 kg liquid TPC have similar sensitivities in that energy range, and that the choice of the target material is not critical, as the larger effective area for a large Z and the better angular resolution for low Z cancel almost exactly in the expression for the sensitivity.

2.3 Momentum measurement

The measurement of the energy of an incoming photon needs information on the momentum p of each electron track. To do so a transition radiation detector (TRD) or a magnetic spectrometer or even worse, as far as the mission mass budget is concerned, an electromagnetic calorimeter has to be used.

But the TPC itself has some measurement potential, as has been used repeatedly (for example in emulsions) since the pioneering works of d’Espagnat [19] and Molière [20]: Given the $1/p$ dependance of the RMS multiple scattering angle, the multiple measurement of angular deflections in the detector provides a measurement of the track momentum.

Here again, the resolution involves contributions from multiple scattering and from the detector resolution. Optimizing the “cell” length on which the measurement is performed, that is, regrouping the TPC sampling in an optimal way, and neglecting conservatively the improvement of the spatial resolution to be expected from the regrouping of several sampling in one cell, we obtain [15] the results presented in Fig. 2 right. As expected the method is useable at low energy ($\sigma_p/p > 0.3$ for $p > 100 \text{ MeV}/c$, over 30 cm in 10 bar argon).

2.4 Polarimetry

Polarimetry, the measurement of the fraction of linear polarization of cosmic sources, is performed for hard X-rays and soft gamma-rays using Compton telescopes, but the sensitivity to polarization is extremely low above 1 MeV [21], due to the asymptotic (at high energy) m/E dependance of the polarization asymmetry [15].

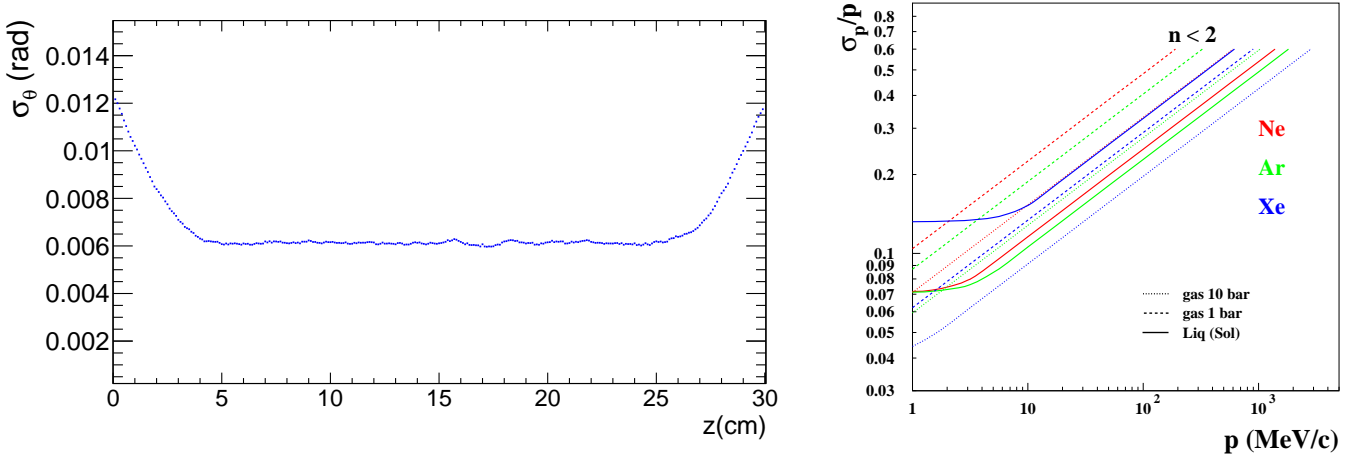


Figure 2: Left: Single track angle RMS uncertainty of a Kalman filter fit from a sample of 5000 simulated 40 MeV/c tracks in 5 bar argon with $\sigma = l = 0.1$ cm; Eqs. (1) predicts an RMS of 12.2 mrad [17]. Right: Relative track momentum resolution for optimal sampling as a function of track momentum for a short TPC (30 cm gas, 10 cm liquid/solid) [15].

2.4.1 Slabs

Hopes to use pair conversion face the hurdle of measuring the azimuthal angle of the conversion plane before multiple scattering ruins this angular information [22, 23, 24, 25]. In a detector formed as a multi-slab series of converter / tracker combinations, multiple scattering in the conversion slab induces an angular deflection of the electron tracks that blurs the azimuthal angle ϕ reconstructed from them. Approximating the two-track opening angle to be equal to the most probable value, produces a dilution¹ D of the polarization asymmetry $D = e^{-2\sigma_\phi^2}$ with $\sigma_\phi \approx 14\sqrt{x/X_0}$, where x is the track pathlength in the slab. [22, 23]. This would lead to the use of slabs with an unrealistically small thickness, that is to an unreasonably large number of tracker layers.

To overcome this difficulty, the use of triplet[26] conversion has been considered: in the case of the conversion of a photon in the electric field of an electron of the detector, the path length of the recoiling electron can be visible in the detector, despite the small recoil energy, thanks to the smallness of the electron mass relative to that of an ion. The azimuthal direction of the recoil carries approximately the same information as the azimuthal angle of the pair plane for polarimetry, but at the cost of the detection and of the reconstruction of very low momentum electrons (check Fig. 3 of Ref. [15]). This has triggered many studies (among which Refs. [29, 30, 28, 31, 32, 33] (and references therein)) since Votruba first computed the differential cross section [27]. But as we shall see [17], the sensitivity to polarimetry of triplet conversion using practical detectors for actual cosmic sources is rather low.

We have studied in detail the parameters that determine the potential of a TPC as a pair-conversion polarimeter in Ref. [17], considering both triplet and “nuclear” conversions, and focusing interest on the MeV – GeV energy range which, in terms of pair-conversion, is the low energy range, but where most of the signal from cosmic sources is expected.

2.4.2 A full, exact, polarized event generator

Most of the photon conversion event generators on the market [35, 34, 32] don’t sample the five-dimensional differential cross section, but instead use a factorized approximation of a 1D or 2D projection of it. Also

¹Note that this expression for the dilution is energy independent: At high energy, the electrons suffer less multiple scattering but the pair’s opening angle decreases as m/E .

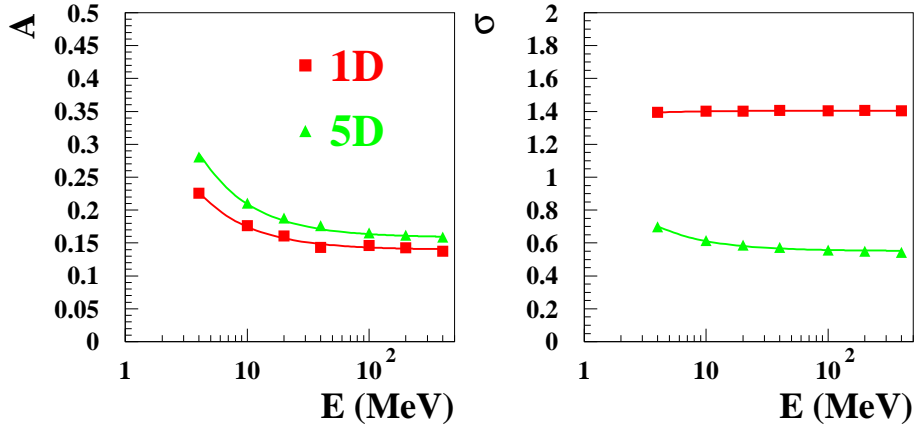


Figure 3: Average (left) and RMS (right) values of the polarization asymmetry without dilution, estimated with a 1D and 5 D optimal variable [17].

low-energy approximations are often used. A number of “polarized” event generators only take polarization into account for lower energy processes such as Compton scattering and the photo-electric effect [36].

We have interfaced the HELAS amplitude calculator [37] with the SPRING event generator [38] to create a full (5-dimensional), exact (down to threshold), polarized event generator, that includes all diagrams either for “nuclear” or for “triplet” conversion. The validation of this event generator w.r.t. 1D distributions published in the past is described to some extent in section 3 of Ref. [17]. (Check, for example, the photon energy variation of the triplet cross section above a recoil momentum threshold (Fig .6 of Ref. [17]) compared to the high-energy asymptotic expression of Ref. [31]). We have also checked the correctness of the amplitude calculation itself by comparison with the Bethe-Heitler (BH) differential cross section [39].

We have explored the actual potential of additional kinematic cuts devised to enlarge the effective value of the polarization asymmetry, an idea that has lead to intense efforts in the past (e.g. [30, 40, 41]). When the loss of statistics induced by the selection is taken into account, the net benefit of applying such a selection, if any, stays minimal. In contrast with polarimeters on man-made accelerator photon beam lines, for which statistics are not an issue [42, 43], for operation in space a high selection efficiency is mandatory.

We have explored the potential of the use of optimal variables, to best extract the information on the polarization contained in the 5D differential cross section. Using a 1D optimal variable doesn’t improve the precision of the measurement of P much, compared to a simple fit of the distribution of the azimuthal angle. In the case of the full 5D optimal variable, the gain in precision is of a factor of about 2 (Fig. 3) at the cost of an increased complexity and of an increased sensitivity to resolution effects.

2.4.3 Polarimetry in a real detector: multiple scattering and optimal fits

We have first studied the traditional “multi-slab” detector geometry with our full event generator, obtaining a dependance of the dilution as a function of the normalized thickness $t \equiv x/X_0$ completely different from the most-probable opening angle value mentioned above ².

We then extend the study to optimal fits. To express the results, we found it interesting to recast eq. (1) into $\sigma_\theta = (p/p_1)^{-3/4}$ with: $p_1 = p_0 \left(\frac{4\sigma^2 l}{X_0^3} \right)^{1/6}$, therefore characterizing a detector, with regard to multiple scattering, by the single parameter p_1 , the “characteristic multiple scattering momentum” of that detector. For example we obtain $p_1 = 50 \text{ keV}/c$ for 1 bar argon, and $p_1 = 1.45 \text{ MeV}/c$ for liquid argon (with here $\sigma = l = 0.1 \text{ cm}$). Due to the $p^{-3/4}$ dependance of the single track angular resolution for optimal fits, the

² Note, though, that intermediate values are similar for the two calculations ($D \approx 1/2$ for $t \approx 10^{-3}$).

dilution is not a constant anymore and gets worse at high energy (Fig. 4 left).

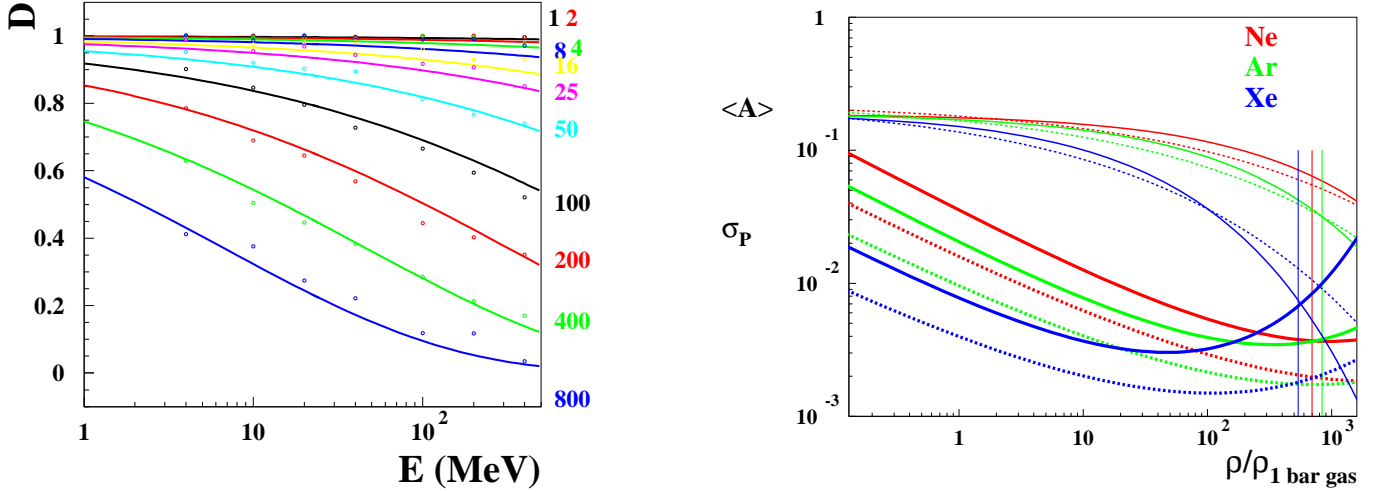


Figure 4: Left: Energy variation of the dilution D of the measurement of P , for various values of the parameter p_1 that parametrize the single-track angular resolution in a thin detector (the values of p_1 (keV) are listed on the right of each plot (1D optimal variable) [17]. Right: Average polarization asymmetry (thin line) and polarization fraction precision (thick line) as a function of detector density normalized to the 1 bar gas density, for a 1 m^3 sensitive volume detector exposed for 1 year and a Crab-like source [17] (nuclear conversion, $\eta = \epsilon = 1$). 1D (solid line) and 5D (dashed line) weight. The vertical lines show the density of the liquid phase.

The precision on a Crab-like source, obtained with a 1 m^3 TPC filled with 5 bar of argon-based gas, with a one full year exposure and 100 % efficiency, would be of 1.0 % (Fig. 4 right). Taking into account minimal kinematical cuts, on the opening angle, on the momentum of each of the two leptons, and on the angular distance to the emitting source, it would increase to 1.4 %.

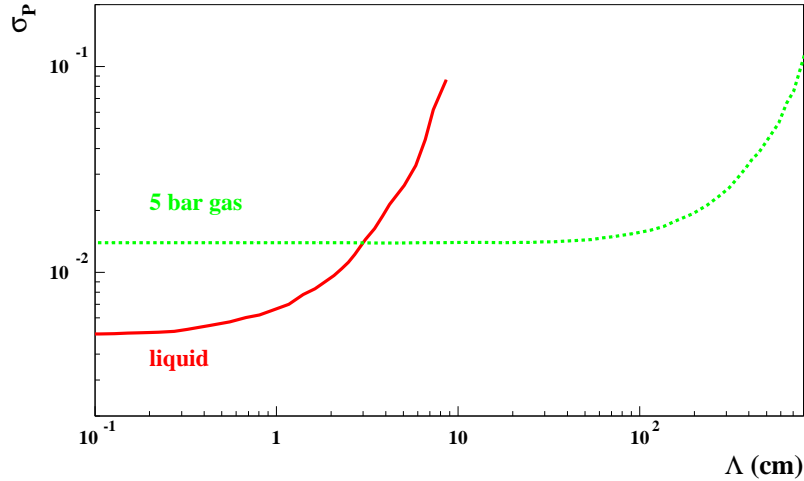


Figure 5: Comparison of the precision σ_P of the measurement of the polarization of a Crab-like source, for a 5 bar gas and a liquid TPC, as a function of the track length limit (1 year, 1 m^3 , exposure fraction $\eta = 1$).

It is clear from Fig. 4 left that performing polarimetry with pair conversions in a dense detector such as a liquid argon TPC [44], a solid neon or silicon TPC, a stack of silicon detectors [45] or a scintillator cube [4] will be extremely difficult, the high value of p_1 making only the very lowest part of the energy

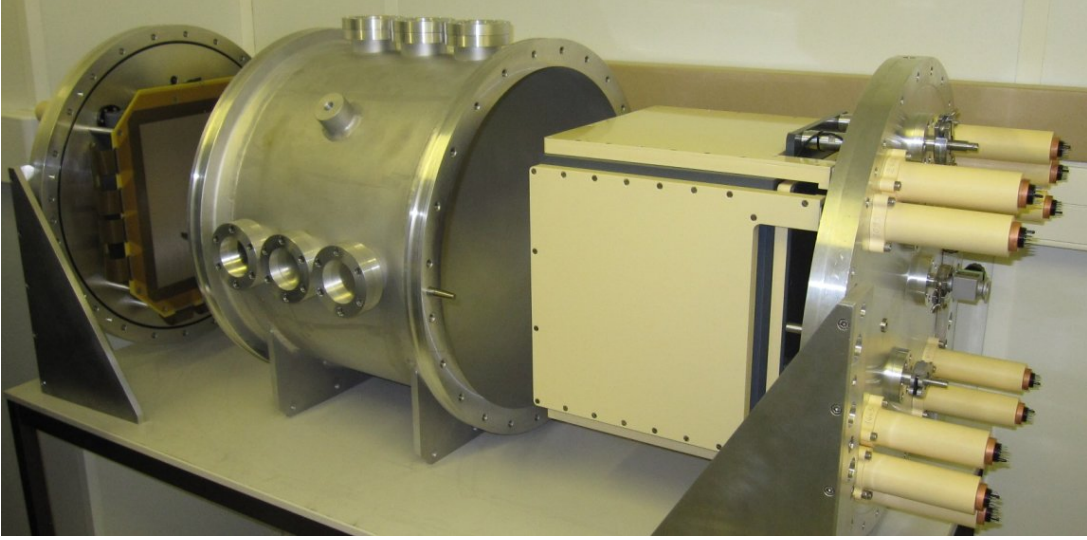


Figure 6: The demonstrator being mounted (2011). From left to right : micromegas, pressure vessel, TPC surrounded by trigger scintillators, PMTs.

spectrum (barely) sensitive to the polarization of the incoming radiation, precisely in the energy range where the angular resolution of these dense detectors is disastrous (almost as bad as that of the Fermi-LAT, see Fig. 1), and the triggerability of the telescope and photon selection from a given source, very problematic. In practice the detector parameter that determines the polarimetric performance of a dense detector is the minimum length Λ for which tracks can be reconstructed: for a liquid-argon TPC to out-perform a 5 bar argon gas TPC would need event detection / trigger / reconstruction with tracks as short as a centimeter (Fig. 5).

The schema of a telescope intended for a space mission is shown in Fig. 13. It consists of a z pile of 3 layers, each layer of 2 back-to-back modules³, with each module having a collection plane segmented into 6×6 $(x, y) = (33 \text{ cm})^2$, $z = 50 \text{ cm}$ blocks. The sensitive volume is 12 m^3 and for a realistic estimate of $\eta \times \epsilon = 0.1$, the sensitivity is close to 1 %. With 2.6 mm wide strips at a 5.2 mm pitch that is 64 channels (one chip) for each direction (x, y) , this \approx one ton telescope would need 432 such chips⁴.

3 HARPO: the experimental project

3.1 The “ground” demonstrator

A “ground” demonstrator was designed in 2010, built in 2011 [46, 47] and tested with cosmic rays in 2012 [48]. The detector is a $(30 \text{ cm})^3$ cubic TPC surrounded with 6 scintillator plates that provide an external trigger. The TPC endplate includes a bulk [49] micromegas [50] amplification system: a metallic mesh is held at 128 μm above a segmented collection plane made of a PCB covered over an instrumented width of 288 mm by two crossed series of 35 μm thick copper strips, each at a pitch of 1 mm. When the mesh is put at a high voltage w.r.t. the collection plane, amplification takes place in the thin space between them. The signals are extracted from the pressure vessel and sampled by the electronics at a rate of $1/(n \times 10 \text{ ns})$, $n > 1$, based on the AFTER chip, that was originally designed for the T2K experiment [53, 51, 52]. It has a DAQ rate limited to $< 180 \text{ Hz}$.

Cosmic-ray tests performed with a “T2K” gas mixture (Ar:95 Isobutane:2 CF₄:3 %), mainly at a pressure

³The back-to-back positioning of two TPC modules, with a thin common metallic grid as a cathode as used for Aleph [59] for example, would here make the handling of the drift high-voltage easier.

⁴The power consumption of that chip, in the present version which is not optimized for space application, is 1 W.

of 2 bar have shown that this demonstrator has excellent tracking properties [48]. After zero-suppression was (optionally) performed in the electronics, data analysis included:

- pixel thresholding;
- pixel clustering;
- track pattern-recognition using combinatorial Hough transform;
- the matching of the (x, t) and (y, t) tracks, based on the close similarity of the time sampling of the same track signal by the two reading systems (along directions x and y);
- track fitting.

3.2 The 2013 upgrade

The 2012 tests have shown that with the 0.4 mm narrow collecting strips that we are using, the micromegas alone does not provide sufficient amplification for routine operation in a safe configuration. We have therefore complemented the micromegas with two layers of Gas Electron Multiplier (GEM) [54]. GEM consist of a 50 μm thick kapton foil with a copper layer on each face and pierced with holes of 70 μm diameter, with a 140 μm pitch. When a high voltage is applied between the two faces, amplification takes place inside the holes.

3.2.1 Test of $\mu\text{M} + \text{GEM}$ combinations with a ^{55}Fe radioactive source

We characterized the combination of a micromegas and of either one or two GEM in a (Ar:95 Isobutane:5 %) gas mixture at atmospheric pressure. This is done in a dedicated test setup, using a ^{55}Fe source[55]. The successive amplification steps are kept at a distance of 2 mm from each other by spacers.

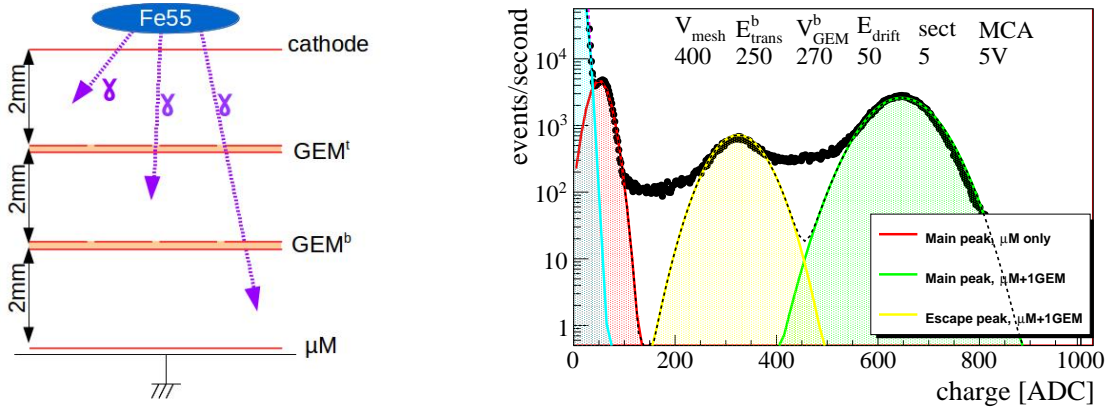


Figure 7: Left: schema of the test set-up. Right: Measured spectrum from a ^{55}Fe source for a $\mu\text{M} + 1 \text{ GEM}$ combination. Three peaks are visible: two ionization peak of ^{55}Fe (main and escape) amplified through one GEM and one micromegas, and the main ionization peak with micromegas amplification only[55].

In argon, the X-rays from a ^{55}Fe source deposit 5.9 keV (main peak) or 2.7 keV (escape peak) in ionization. This conversion can happen either above or below a given GEM sheet. The ionization electrons are therefore amplified by that GEM or not. A typical measured spectrum is shown in Fig. 7 right, where we can see the main and escape peaks with amplification from the micromegas and one GEM, and the main peak with micromegas amplification only. The ratio of the two main peaks provides a precise measurement of the absolute GEM amplification gain. These measurements are used to test the dependence of the gain with

the values of the electric fields in the setup. Figure 8 shows that the amplification gain grows exponentially with the voltage applied for both the micromegas and the GEM. Moreover, the slope is independent of the other parameters.

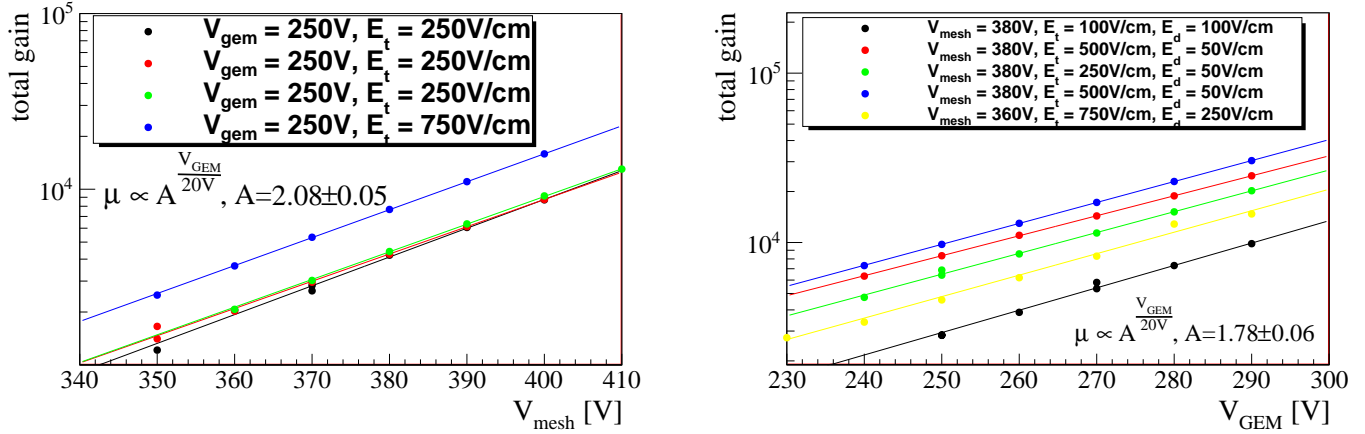


Figure 8: Characterization of a $\mu\text{M} + 2$ GEM combination in a 1 bar (Ar:95 Isobutane 5 %) gas mixture and X-rays from a ^{55}Fe radioactive source[55].

The effective gain of the amplification chain depends also on the “transfer” electric field on each side of the GEM and above the micromegas. This is usually described as transparency ($\mathcal{T}_{\mu\text{M}}$) for micromegas, and collection (\mathcal{C}_{GEM}) and extraction (\mathcal{E}_{GEM}) efficiency for GEM. At a fixed amplification voltage, we can assume that the micromegas transparency and the GEM collection efficiency depend on the value of the electric field above the amplification system considered, while the GEM extraction efficiency depends on the value of the field below the GEM. The respective gains can then be decomposed as follows:

$$g_{\mu\text{M}}^{\text{effective}} = g_{\mu\text{M}}(V_{\mu\text{M}}) \times \mathcal{T}_{\mu\text{M}}(E_{\text{above}}) \quad (2)$$

$$g_{\text{GEM}}^{\text{effective}} = \mathcal{E}_{\text{GEM}}(E_{\text{below}}) \times g_{\text{GEM}}(V_{\text{GEM}}) \times \mathcal{C}_{\text{GEM}}(E_{\text{above}}) \quad (3)$$

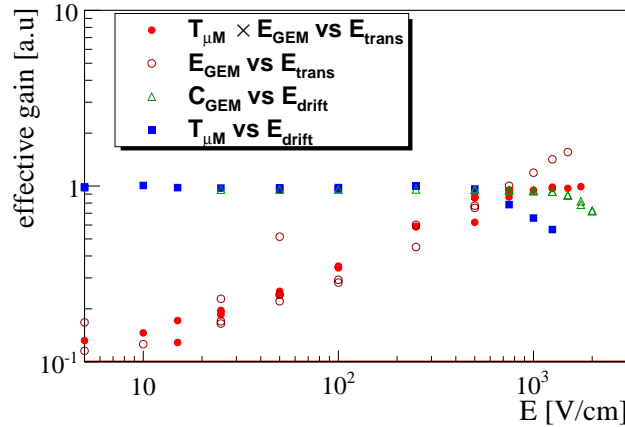


Figure 9: Measurement of the micromegas transparency \mathcal{T} and of the GEM collection \mathcal{C} and extraction \mathcal{E} efficiencies as a function of the relevant electric field[55]. The normalisation is arbitrary.

By measuring the gain variations with each of the fields, we can extract these three parameters (Fig 9). The micromegas transparency \mathcal{T} and GEM collection \mathcal{C} show a clear plateau, that probably corresponds to 100%. The GEM extraction does not reach a plateau on the field range that we have explored, and therefore we can’t determine the absolute scale of the GEM transparency.

3.2.2 Cosmic ray tests of the up-graded demonstrator

The $\mu\text{M} + 2$ GEM was commissioned into the TPC and the full detector was tested with cosmic rays, using the same gas mixture. Measurements of the energy deposit of tracks traversing the full length of the TPC enable to evaluate the effective gain of the amplification system. Fig. 10 shows the dependence of the gain with the voltage applied on the GEM and micromegas, for several gas pressures. The expected exponential behavior is confirmed.

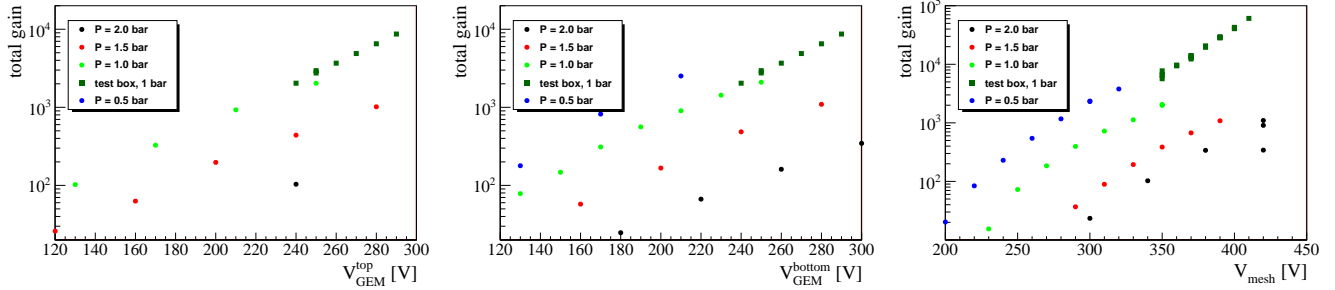


Figure 10: Gain in the HARPO TPC evaluated from traversing cosmic ray tracks[55].

The test-box measurements and the TPC tests were performed with the same μM and GEMs but with two completely different electronics systems, that were calibrated separately. It is therefore interesting to note that the variations of the signal with V_{GEM} (Fig. 10 left and center) at 1 bar show an agreement within $\approx 10\%$ between them. At the highest value of the total gain, some saturation effects are clearly visible (Fig. 10 right); their correction is still under study.

Event reconstruction is documented in Fig. 11. The calibration of the TPC, i.e. the measurement of the trigger time t_0 and of the drift velocity v_{drift} that take part in the basic relation of the TPC mechanism, $z = v_{\text{drift}}(t - t_0)$, is performed easily with “through” tracks, that is with cosmic rays that cross the full z thickness of 30 cm (Fig. 12). The low electron absorption rate of 10 ms^{-1} along the track is visible. The combination of the values of the drift velocity and of the digitization sampling rate, and the trigger delay are set so that the “physical” signal from the TPC extend from time bin 100 to bin 400, so that both in the transverse (x, y) and in the longitudinal (z) directions, the TPC is sampled with the same pitch of 1 mm.

The upgrade of the electronics includes the use of the recently developed Feminos[63] back-end cards and of the PMm2 trigger card [64] based of the PARISROC chip[65].

4 Perspectives

Short term 2014. We are presently finalizing the demonstrator set-up, with the goal of characterizing it in a beam of polarized gamma rays at NewSUBARU[57] in the energy range 2 - 76 MeV in the fall of this year 2014.

Longer term. We plan to develop the spatialization of the TPC technology, with in particular studies of:

- **Triggerability.** A limitation of the present electronics based on the AFTER chip is the need of an external trigger – at the moment provided by the combination of signals from scintillators. We will replace these chips by the new generation, self-triggerable member of the same family: the AGET chip [58] that has been tested successfully recently. The full use of the real time information provided by the chip during the drift of the electrons in the gas ($\approx 5 \mu\text{s}$) should allow us to build an efficient trigger much faster than the digitization time $\mathcal{O}(\text{ms})$.

- **Clean technology.** In the present “ground” demonstrator, most of the detector components (TPC field cage, PCB, scintillators, wavelength shifter bars .. glue ..) are located inside the same sealed pressure vessel, without any gas purification. As a consequence, after a month of running, the TPC

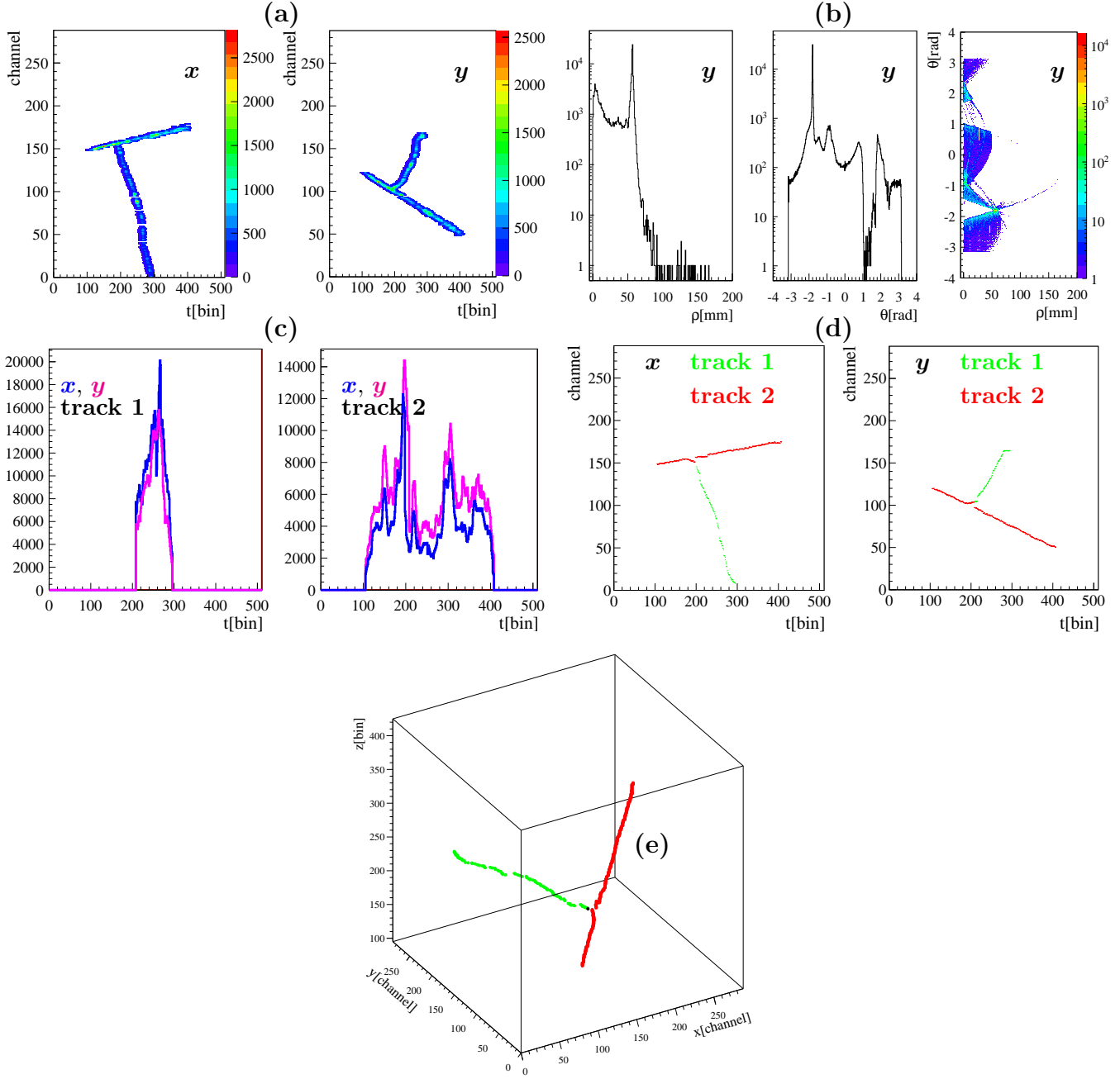


Figure 11: Display of an event in the μ M + 2 GEM detector configuration with a 2 bar (Ar:95 Isobutane 5 %) gas mixture. The TPC was positioned “vertically”, with cosmic rays entering it from above through the amplification system. A cosmic ray crosses through the full TPC thickness (30cm), leaving a lower energy electron (δ ray). The trigger time for this run was $t_0 \approx 100$ bin. (a) The two event “maps” (x, t) and (y, t) after pedestal subtraction and thresholding (a thin space without any signal is visible due to the presence of a spacer). (b) The distributions of the ρ, θ variables that parametrize a track in the combinatorial Hough track pattern recognition[48, 56] and their scatter plot. (c) The time spectra for the two tracks, for direction x and y , which are used to perform x, y track matching. (d) The maps of the clusters associated with the two matched tracks. (e) A 3D view of the reconstructed event, with vertexing (the vertex is indicated by the black dot) [56].

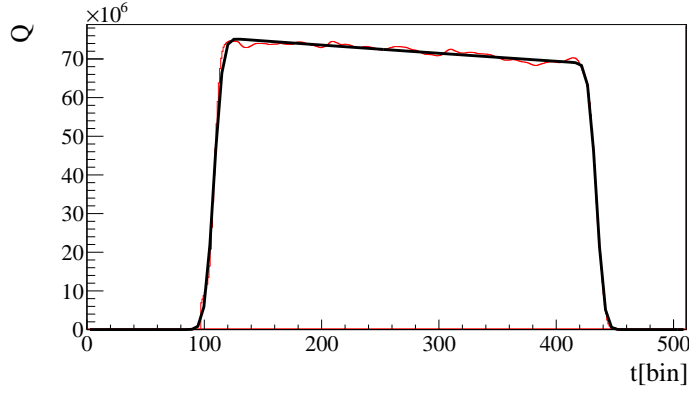


Figure 12: Cumulative time spectrum (in ADC “counts”) of traversing tracks of a run of 5000 events, in a (Ar:95 Isobutane:5 %) gas mixture at a pressure of 1.52 bar and with a sampling of 30 ns and a shaping of 100 ns (Ref. [56]).

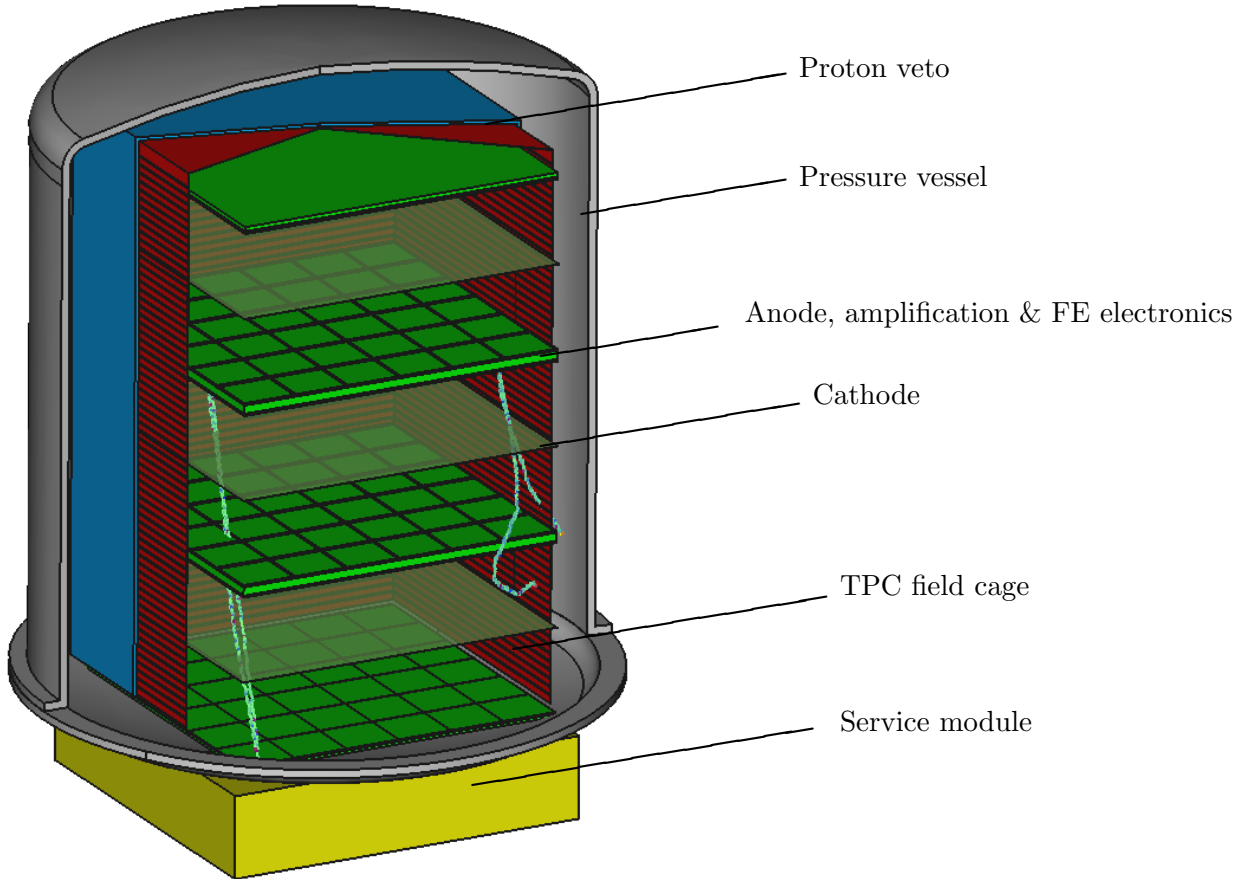


Figure 13: Exploded schematic view of a flight telescope consisting of 3 layers, each layer of 2 back-to-back modules, each module a $(2\text{ m})^2 \times 0.5\text{ m}$ TPC with an endplate segmented into $(33\text{ cm})^2$ micromegas and charge collection blocks. Conversions of a 100 MeV (left) and of a 10 MeV (right) photon in the TPC gas.

showed a significant absorption of the drifting electrons along their path through the full length. The use of a TPC in space will need to maintain the gas to a high purity for several years.

Besides the standard use of purification of recirculated gas, the content of the pressurized vessel could be split into two (series of) separate volumes, a “clean” volume dedicated only to drift and amplification, and a “dirty” part that contains all the rest, strip PCB, front-end electronics (FE) ..

The signal is read by its capacitive coupling through a dielectric layer as for the Aleph calorimeter [59] or in the “Piggyback” technology that has been validated recently [60].

- **Small gaps for high pressure operation.** Last but not least, the optimization of the sensitivity to faint sources and to polarization at a given limit volume encourages to use high-pressure detectors. As the maximum of the micromegas gain is reached at a pressure that increases when the micromegas gap size is decreased [61], we are developing small gap “micro-bulk” detectors [62].

Acknowledgments

It is our pleasure to acknowledge contributions from Leszek Ropelewski *et al.* (RD51 lab at CERN) for the commissioning of the GEM, Eric Delagnes and Denis Calvet (Irfu) for their help in using the T2K electronics, Eric Wanlin (IPNO) for his support on the PMm2 trigger card and Shuji Miyamoto (LASTI) for his continued support in the preparation of the data taking at NewSUBARU.

This work is funded by the P2IO LabEx (ANR-10-LABX-0038) in the framework “Investissements d’Avenir” (ANR-11-IDEX-0003-01) managed by the French National Research Agency (ANR), and directly by the ANR (ANR-13-BS05-0002).

5 Notes added in proof

During the conference I profited from many discussions relevant to this paper:

- Keith Jahoda [66] pointed me to a study [67] that demonstrated the feasibility of a TPC detector with a lifetime on the 20 year scale for the GEMS project;
- Eric Charles insisted on the need to improve the angular resolution in the $< 1\text{GeV}$ energy range in his post-Fermi “lessons learned” talk [68];
- Meng Su presented the PANGU project [69]. One of its options is a stack of silicon detectors without any high Z converter which, in contrast with previous works, deliberately attempts to perform polarimetry by the use of thin ($150\text{ }\mu\text{m}$) wafers. Indeed, in the approximation of hyper-thin wafers spaced at a large enough distance, such a stack would become equivalent to a low density homogeneous detector, and the formalism of Refs. [15, 17] would apply.

References

- [1] V. Schönfelder, *Lessons learnt from COMPTEL for future telescopes*, New Astr. Rev. **48** (2004) 193
- [2] M. Ackermann *et al.* [Fermi-LAT Collaboration], *The Fermi Large Area Telescope On Orbit: Event Classification, Instrument Response Functions, and Calibration*, Astrophys. J. Suppl. **203**, 4 (2012) [arXiv:1206.1896 [astro-ph.IM]].
- [3] J. Greiner *et al.*, *GRIPS - Gamma-Ray Imaging, Polarimetry and Spectroscopy*, Exper. Astron. **34**, 551 (2012) [arXiv:1105.1265 [astro-ph.HE]].
- [4] F. Lebrun *et al.*, *The Gamma Cube: a novel concept of gamma-ray telescope*, this conference, Paper 9144-10
- [5] AstroMeV Consortium, <http://astromev.in2p3.fr/>
- [6] T. Piran, *Gamma-ray bursts and the fireball model*, Phys. Rept. **314**, 575 (1999). [astro-ph/9810256].
- [7] E. Waxman, *New direction for gamma-rays*, Nature **423**, 388 (2003). [astro-ph/0305414].
- [8] J. Granot, A. Konigl, *Linear polarization in GRB afterglows: the case for an ordered magnetic field*, Astrophys. J. **594**, L83 (2003). [astro-ph/0304286].

- [9] D. Eichler, A. Levinson, *Polarization of GRB via scattering off a relativistic sheath*, *Astrophys. J.* **596**, L147 (2003). [astro-ph/0306360].
- [10] M. Lyutikov, V. I. Pariev, R. D. Blandford, *Polarization of prompt GRB emission: Evidence for electromagnetically - dominated outflow*, *Astrophys. J.* **597**, 998 (2003). [astro-ph/0305410].
- [11] H. Zhang and M. Böttcher, *X-Ray and Gamma-Ray Polarization in Leptonic and Hadronic Jet Models of Blazars*, *Astrophys. J.* **774**, 18 (2013) [arXiv:1307.4187 [astro-ph.HE]].
- [12] T. Jacobson, S. Liberati and D. Mattingly, *Lorentz violation at high energy: Concepts, phenomena, and astrophysical constraints*, *Ann. Phys.*, 321 (2006) 150
- [13] R. L. Gluckstern, *Uncertainties in track momentum and direction, due to multiple scattering and measurement errors*, *Nucl. Instrum. Meth.* **24**, 381 (1963).
- [14] W. R. Innes, *Some formulas for estimating tracking errors*, *Nucl. Instrum. Meth. A* **329**, 238 (1993).
- [15] D. Bernard, *TPC in gamma-ray astronomy above pair-creation threshold*, *Nucl. Instrum. Meth. A* **701**, 225 (2013) [Erratum-ibid. A **713**, 76 (2013)] [arXiv:1211.1534 [astro-ph.IM]].
- [16] J. Beringer *et al.* [Particle Data Group Collaboration], *Review of Particle Physics*, *Phys. Rev. D* **86**, 010001 (2012).
- [17] D. Bernard, *Polarimetry of cosmic gamma-ray sources above e^+e^- pair creation threshold*, *Nucl. Instrum. Meth. A* **729**, 765 (2013) [arXiv:1307.3892 [astro-ph.IM]].
- [18] R. Frühwirth, *Application of Kalman filtering to track and vertex fitting*, *Nucl. Instrum. Meth. A* **262**, 444 (1987).
- [19] B. d'Espagnat, *Mesure de la diffusion des traces dans les émulsions : élimination de la diffusion parasite*, *Comptes rendus de l'Académie des sciences* 232 (1951) 800.
- [20] G. Molière, *Theorie der Streuung schneller geladener Teilchen. III. Die Vielfachstreuung von Bahns Spuren unter Berücksichtigung der statistischen Kopplung*, *Zeitschrift Naturforschung A*, 10 (1955) 177.
- [21] M.L. McConnell, J.M. Ryan, *Status and prospects for polarimetry in high energy astrophysics*, *New Astr. Rev.* **48** (2004) 215.
- [22] Yu. D. Kotov, *Methods of measurement of gamma-ray polarization*, *Space Science Reviews* **49** (1988) 185.
- [23] Mattox, J. R., Mayer-Hasselwander, H. A., Strong, A. W., *Analysis of the COS B data for evidence of linear polarization of VELA pulsar gamma rays*, *Astrophys. J.* 363 (1990) 270.
- [24] P. F. Bloser, S. D. Hunter, G. O. Depaola and F. Longo, *A Concept for a high-energy gamma-ray polarimeter*, astro-ph/0308331.
- [25] S. D. Hunter *et al.*, *A Pair Production Telescope for Medium-Energy Gamma-Ray Polarimetry*, *Astropart. Phys.* **59** (2014) 18 [arXiv:1311.2059 [astro-ph.IM]].
- [26] F. Perrin, *Possibilité de matérialisation par interaction d'un photon et d'un électron*, *Compt. Rend.* **197** (1933) 1100.
- [27] V. Votruba, *Pair production by gamma-rays in the field of an electron*, *Bull. Int. Acad. Tchèque Sci.* **49** (1948) 19.
- [28] V. F. Boldyshev *et al.*, *Measurement of photon beam linear polarization using asymmetry of the recoil electrons from the photoproduction of e^+e^- pairs on electrons*, *Phys. Part. Nucl.* **25**, 292 (1994).
- [29] K. S. Suh and H. A. Bethe, *Recoil Momentum Distribution in Electron Pair Production*, *Phys. Rev.* **115** 672 (1959).
- [30] I. Endo and T. Kobayashi, *Exact evaluation of triplet photoproduction*, *Nucl. Instrum. Meth. A* **328**, 517 (1993).
- [31] M. L. Iparraguirre and G. O. Depaola, *Pair production by gamma-rays on electrons. Threshold for the momentum recoil detection*, *Eur. Phys. J. C* **71**, 1778 (2011).
- [32] G. O. Depaola and M. L. Iparraguirre, *Angular distribution for the electron recoil in pair production by linearly polarized gamma-rays on electrons*, *Nucl. Instrum. Meth. A* **611**, 84 (2009).
- [33] M. L. Iparraguirre and G. O. Depaola, *About electrons in Triplet Production*, arXiv:1406.3001 [hep-ph].
- [34] G. O. Depaola, *Azimuthal distribution for pair production by high-energy gamma-rays*, *Nucl. Instrum. Meth. A* **452** (2000) 298.
- [35] A. F. Bielaiew, *Improved angular sampling for pair production in the EGS4 code system*, NRCC Report: PIRS-0287R.

- [36] G. A. P. Cirrone *et al.*, *Validation of the Geant4 electromagnetic photon cross-sections for elements and compounds*, Nucl. Instrum. Meth. A **618** (2010) 315.
- [37] H. Murayama, I. Watanabe and K. Hagiwara, *HELAS: HELicity amplitude subroutines for Feynman diagram evaluations*, KEK-91-11.
- [38] S. Kawabata, *A New version of the multidimensional integration and event generation package BASES/SPRING*, Comput. Phys. Commun. **88**, 309 (1995).
- [39] “The quantum theory of radiation”, W. Heitler, 1954.
- [40] J. Asai and D.M Skopik, *Asymmetry ratio in pair production and the degree of linearly polarized photons at intermediate energies*, Nucl. Instrum. Meth. A **432** (1999) 195.
- [41] F. Adamyan *et al.*, *Experimental study of photon beam polarimeter based on nuclear e^+e^- pair production in an amorphous target*, Nucl. Instrum. Meth. A **579**, 973 (2007) [physics/0610112].
- [42] C. de Jager *et al.*, *A Pair Polarimeter for Linearly Polarized High Energy Photons*, Eur. Phys. J. A **19**, S275 (2004) [physics/0702246 [PHYSICS]].
- [43] B. Wojtsekhowski, D. Tedeschi and B. Vlahovic, *A Pair polarimeter for linearly polarized high-energy photons*, Nucl. Instrum. Meth. **515**, 605 (2003).
- [44] G. A. Caliendo *et al.*, *A new concept of γ -ray telescope. LArGO: Liquid Argon Gamma-ray Observatory*, arXiv:1312.4503 [astro-ph.IM].
- [45] A. Morselli *et al.*, *GAMMA-LIGHT: High-Energy Astrophysics above 10 MeV*, Nuclear Physics B Proc. Supp. **239** **240** 2013 193. [arXiv:1406.1071 [astro-ph.IM]].
- [46] D. Bernard, *High-angular-precision gamma-ray astronomy and polarimetry above the pair-creation threshold*, 2nd International Conference on Micro Pattern Gaseous Detectors 29 Aug - 1 Sept 2011, Kobe, Japan, JINST **7**, C03029 (2012).
- [47] D. Bernard and A. Delbart, *High-angular-precision gamma-ray astronomy and polarimetry*, 6th International Conference On New Developments In Photodetection 4-8 Jul 2011, Lyon, France, Nucl. Instrum. Meth. A **695**, 71 (2012)
- [48] D. Bernard, *HARPO - A Gaseous TPC for High Angular Resolution Gamma-Ray Astronomy and Polarimetry from the MeV to the TeV*, Nucl. Instrum. Meth. A **718**, 395 (2013)
- [49] I. Giomataris *et al.*, *Micromegas in a bulk*, Nucl. Instrum. Meth. A **560**, 405 (2006)
- [50] Y. Giomataris, P. Rebourgeard, J. P. Robert and G. Charpak, *MICROMEGAS: A high-granularity position-sensitive gaseous detector for high particle-flux environments*, Nucl. Instrum. Meth. A **376**, 29 (1996).
- [51] P. Baron *et al.*, *Architecture and Implementation of the Front-End Electronics of the Time Projection Chambers in the T2K Experiment*, IEEE Trans. Nucl. Sci. **57** (2009) 406.
- [52] D. Calvet *et al.*, *The Back-end Electronics of the Time Projection Chambers in the T2K Experiment*, IRFU-10-77, Presented at IEEE 17th Real Time Conference, Lisboa, Portugal, 24-28 May 2010.
- [53] P. Baron, D. Calvet, E. Delagnes *et al.*, *AFTER, an ASIC for the readout of the large T2K time projection chambers*, IEEE Trans. Nucl. Sci. **55**, 1744 (2008).
- [54] F. Sauli, *GEM: A new concept for electron amplification in gas detectors*, Nucl. Instrum. Meth. A **386**, 531 (1997).
- [55] Ph. Gros, *Characterisation of a micromegas + 2 GEM assembly for HARPO*, 13th RD51 Collaboration Meeting, CERN 5 - 7 Feb 2014.
- [56] Shaobo Wang, Ph D thesis, work in progress.
- [57] S Amano *et al.*, *Several-MeV γ -ray generation at NewSUBARU by laser Compton backscattering*, Nucl. Instrum. Meth. A **602** 2009 337.
NewSUBARU is a facility operated by LASTI, the Laboratory of Advanced Science and Technology for Industry of University of Hyogo, Japan.
- [58] S. Anvar, P. Baron *et al.*, *AGET, the GET front-end ASIC, for the readout of the Time Projection Chambers used in nuclear physic experiments*, Nuclear Science Symposium and Medical Imaging Conference (NSS/MIC), 2011 IEEE 745 - 749.

- [59] D. Decamp *et al.* [ALEPH Collaboration], *ALEPH: A detector for electron-positron annihilations at LEP*, Nucl. Instrum. Meth. A **294**, 121 (1990) [Erratum-ibid. A **303**, 393 (1991)].
- [60] D. Attié *et al.*, *Piggyback resistive Micromegas*, JINST **8**, C11007 (2013) [arXiv:1310.1242 [physics.ins-det]].
JINST **8**, P05019 (2013) [arXiv:1208.6525 [physics.ins-det]].
- [61] D. Attié *et al.*, *Towards smaller gap microbulks*, JINST **9**, C04013 (2014).
- [62] S. Andriamonje, D. Attié *et al.*, *Development and performance of Microbulk Micromegas detectors*, JINST **5**, P02001 (2010).
- [63] D. Calvet, *A Versatile Readout System for Small to Medium Scale Gaseous and Silicon Detectors*, IEEE Trans. Nucl. Sci. **61** (2014) 675.
- [64] B. Genolini *et al.*, *PM2: Large photomultipliers and innovative electronics for the next-generation neutrino experiments*, Nucl. Instrum. Meth. A **610** (2009) 249 [arXiv:0811.2681 [physics.ins-det]].
- [65] S. Conforti Di Lorenzo *et al.*, *PARISROC, an autonomous front-end ASIC for triggerless acquisition in next generation neutrino experiments*, Nucl. Instrum. Meth. A **695** (2012) 373.
- [66] Joanne E. Hill *et al.*, *Design improvements and x-ray performance of a time projection chamber polarimeter for persistent astronomical sources*, This conference, [9144-58].
- [67] Joanne E. Hill *et al.*, *Lifetime estimation of a time projection chamber x-ray polarimeter*, Proc. SPIE 8859, UV, X-Ray, and Gamma-Ray Space Instrumentation for Astronomy XVIII, 25 - 29 August 2013, San Diego USA.
- [68] Eric Charles *et al.*, *Scientific motivations and technical design considerations for future high-energy gamma-ray telescopes in light of lessons learned from the Fermi Mission*, This conference, [9144-13].
- [69] Meng Su *et al.*, *PANGU: a high resolution Gamma-ray Space telescope*, This conference, [9144-130] and arXiv:1407.0710 [astro-ph.IM].

Contents

1	INTRODUCTION	1
1.1	Angular resolution	1
1.2	Polarimetry	2
2	HARPO: a TPC as a gamma-ray telescope and polarimeter	3
2.1	Angular resolution	3
2.2	Conversion efficiency, effective area	3
2.3	Momentum measurement	4
2.4	Polarimetry	4
2.4.1	Slabs	5
2.4.2	A full, exact, polarized event generator	5
2.4.3	Polarimetry in a real detector: multiple scattering and optimal fits	6
3	HARPO: the experimental project	8
3.1	The “ground” demonstrator	8
3.2	The 2013 upgrade	9
3.2.1	Test of $\mu\text{M} + \text{GEM}$ combinations with a ^{55}Fe radioactive source	9
3.2.2	Cosmic ray tests of the up-graded demonstrator	11
4	Perspectives	11
5	Notes added in proof	14